

# Visible Light-Induced Degradation of Inverted Polymer: Nonfullerene Acceptor Solar Cells: Initiated by the Light Absorption of ZnO Layer

Bowen Liu, Yunfei Han, Zerui Li, Huimin Gu, Lingpeng Yan, Yi Lin, Qun Luo,\*  
Shangfeng Yang, and Chang-Qi Ma\*

Power conversion efficiencies (PCEs) of polymer solar cells (PSCs) have exceeded 18% in the last few years. Stability has therefore become the next most important issue before commercialization. Herein, the degradation behaviors of the inverted PM6:IT-4F (PBDB-T-2F:3,9-bis(2-methylene-(3-(1,1-dicyanomethylene)-6,7-difluoro)indanone))-5,5,11,11-tetrakis(4-hexylphenyl)-dithieno[2,3-*d*:2',3'-*d'*]-*s*-indaceno[1,2-*b*:5,6-*b'*]dithiophene) solar cells with different ZnO layers are systematically investigated. The PCE decay rates of the cells and the photo-bleaching process of the IT-4F containing organic films on ZnO surface are directly correlated with the light-absorption ability of the ZnO layer in the visible light range, indicating that photochemical decomposition of IT-4F is initiated by the light absorption of ZnO layer. By analyzing the products of the aged ZnO/IT-4F films with matrix-assisted laser desorption ionization time-of-flight mass spectrometry (MALDI-TOF-MS), it is confirmed that photochemical reactions at the IT-4F/ZnO interface include de-electron-withdrawing units and dealkylation on the side-phenyl ring. Hydroxyl radicals generated by the photo-oxidation of dangling hydroxide by ZnO are confirmed by electron spin resonance (ESR) spectroscopy measurements, which is attributed as the main reason causing the decomposition of IT-4F. Surface treatment of ZnO with hydroxide and/or hydroxyl radical scavenger is found to be able to improve the stability of the PSCs, which further supports the proposed degradation mechanism.

## 1. Introduction

Polymer solar cells (PSC) have the advantages of light-weight, flexibility, and solution processability that ensure high throughput production of PSCs with roll-to-roll printing processes.<sup>[1]</sup> In recent years, new nonfullerene electron acceptors (NFA) were developed and have become the focus of research because of the significant breakthroughs in the power conversion efficiency (PCE) of PSC.<sup>[2]</sup> Compared to the fullerene derivatives, the NFA exhibit several advantages, including ease of chemical synthesis, readily tunable energy levels, and enhanced light absorption over the visible to near IR range.<sup>[3]</sup> To date, high PCE of 18% was achieved recently for NFA-based solar cells, demonstrating the great application prospective of PSCs.<sup>[4]</sup>

As an equally important factor in the commercialization of PSC, the stability of PSCs lagged far behind the efficiency optimization.<sup>[5]</sup> There have been many studies on the degradation of NFA-based solar cells, and most of them have focused on the degradation mechanisms related to the active layer and device architecture.<sup>[6]</sup>

B. Liu, Y. Han, Z. Li, H. Gu, Dr. L. Yan, Prof. Q. Luo, Prof. C.-Q. Ma  
Printable Electronics Research Center  
Suzhou Institute of Nano-Tech and Nano-Bionics  
Chinese Academy of Sciences  
Ruoshui Road 398, SEID, SIP, Suzhou 215123, P. R. China  
E-mail: qluo2011@sinano.ac.cn; cqma2011@sinano.ac.cn


B. Liu  
Nano Science and Technology Institute  
University of Science and Technology of China  
166 Ren Ai Road, SEID SIP, Suzhou, Jiangsu 215123, P. R. China

Y. Han, Z. Li, Prof. Q. Luo, Prof. C.-Q. Ma  
College of Nano-Tech and Nano-Bionics  
University of Science and Technology of China  
Hefei 230027, P. R. China

H. Gu, Dr. L. Yan  
Key Laboratory of Interface Science and Engineering in Advanced Materials  
Ministry of Education  
Taiyuan University of Technology  
79 Yingze Street, Taiyuan 030024, P. R. China

Prof. Y. Lin  
Department of Chemistry  
Xi'an Jiaotong Liverpool University  
Renai Road 11, SEDI, SIP, Suzhou 215123, P. R. China

Prof. S. Yang  
CAS Key Laboratory of Materials for Energy Conversion  
Department of Materials Science and Engineering  
University of Science and Technology of China  
Hefei 230026, P. R. China

 The ORCID identification number(s) for the author(s) of this article can be found under <https://doi.org/10.1002/solr.202000638>.

DOI: 10.1002/solr.202000638

Among which, Brabec and co-workers demonstrated that photostability of polymer:NFA cells is strongly dependent on the end-group of the terminal accepting moieties of the A-D-A type NFAs, and fluorination of the end-group stabilizes molecules against light soaking, whereas methyl groups show an opposite trend.<sup>[6d]</sup> In another article, the same research group revealed that the UV-induced degradation of both fullerene and NFA cells are highly related to the use of 1,8-diiodooctane (DIO) additive, which underwent photochemical reactions of acceptor molecules with the DIO radicals generated under UV light illumination.<sup>[6e]</sup> Kim and co-workers investigated the role of molecular structure and conformation on the photostability of the materials in the air, and results demonstrated that a planar structure of the conjugated backbone is important for stability.<sup>[6f]</sup> Zhu and co-workers reported that during the aging of polymer:NFA solar cells, the active layer undergoes a continuous vertical phase-separation process, forming a polymer-rich top surface and NFA-rich bottom surface. It accelerates the reaction of hole-transporting layer and NFA, which in turn causes the performance decay of solar cells, and using of the inverted configuration device can significantly improve the device stability.<sup>[6g]</sup> These excellent pioneering research works demonstrated the undesired photochemical reaction of the NFA acceptors within the photoactive layer cause the decomposition of NFA molecules, which consequently decreases the device performance.

In addition to the degradation of NFA molecules within the photoactive layer, interface interactions between the electron transport layer (ETL) and the NFA molecules were recently recognized to be another important reason for the PSC performance decay. Zhou and co-workers first reported the photobleaching of the 3,9-bis(2-methylene-((3-(1,1-dicyanomethylene)-6,7-difluoro)indanone))-5,5,11,11-tetrakis(4-hexylphenyl)-dithieno[2,3-*d*:2',3'-*d'*]-s-indaceno[1,2-*b*:5,6-*b'*]dithiophene (IT-4F) film on ZnO surface under UV light illumination. This was attributed to be the decomposition of the C=C ethynyl group of IT-4F, as confirmed by the mass spectrometry (MS) results.<sup>[7]</sup> Similarly, Park and Son reported that 3,9-bis(2-methylene-((3-(1,1-dicyanomethylene)-indanone))-5,5,11,11-tetrakis(4-hexylphenyl)-dithieno[2,3-*d*:2',3'-*d'*]-s-indaceno[1,2-*b*:5,6-*b'*]dithiophene (ITIC, the IT-4F analogous) also undergoes UV photobleaching on the ZnO surface. With the MS analyses of the by-products of photobleached thin film, the authors proposed a degradation mechanism of photochemical decomposition of ITIC by hydroxyl radicals ( $\cdot\text{OH}$ ).<sup>[8]</sup> However, no direct evidence for the formation of  $\cdot\text{OH}$  was provided. Very recently, Yip and co-workers reported that the lifetime of the poly[4,8-bis(5-(2-ethylhexyl)thiophen-2-yl)benzo[1,2-*b*:4,5-*b'*]dithiophene-alt-3-fluorothien-2-yl]thiophene-2-carboxylate];(2,2'-((2Z,2'Z)-((4,4,9,9-Tetrakis(4-hexylphenyl)-4,9-dihydro-sindaceno[1,2-*b*:5,6-*b'*]dithiophene-2,7-diyl)bis(4-((2ethylhexyl)oxy)thiophene-5,2-diyl))bis(methanylylidene))bis(5,6-difluoro-3-oxo-2,3-dihydro-1*H*-indene-2,1-diylidene))dimalononitrile (PTB7-Th:IEICO-4F) cells can be dramatically improved after surface treatment of ZnO layer with a self-assembled fullerene monolayer (C<sub>60</sub>-SAM), demonstrating that interface interaction between ETL and photoactive layer plays a key role in influencing the device stability.<sup>[9]</sup> However, no degradation mechanism was provided in this article.

These literature reports clearly confirmed that the interfacial photochemical reaction between ZnO and NFA happened under

UV light illumination. Knowing that the photoactive layer of a PSC also absorbs both UV and visible light under operation, it is therefore highly interesting to know whether light absorption of the photoactive layer is involved in the degradation of the cells or not. In the meanwhile, it is still not clear as to the reactive species that cause the decomposition of the acceptor. In this article, we investigated the influence of ZnO layer on the degradation behaviors of the high-performance PM6:IT-4F solar cells under light-emitting diode (LED) white-light illumination. Our experiments found that the PM6:IT-4F cells decay much faster when the ZnO layer absorbs more visible light. In addition, photobleaching was only found for the organic films containing IT-4F. These experimental results confirm that light absorption of ZnO is the key step causing the solar-cell degradation. Electron spin resonance (ESR) on the ZnO film and the Matrix-Assisted Laser Desorption Ionization Time-Of-Flight Mass Spectrometry (MALDI-TOF-MS) analysis on the products of the ZnO/NFA films further confirm the formation of hydroxyl radicals; even the annealed ZnO film is illuminated inside the glovebox. Based on these findings, we proposed that light-induced interface degradation processes of the polymer:NFA solar cells involve the formation of ZnO excitons through the absorption of photons by ZnO, and the following oxidation of hydroxide to hydroxyl radicals, which decomposes the NFA molecules. With the understanding of the degradation mechanism, treatment of the ZnO surface with hydroxide and/or hydroxyl radical scavenger successfully improves the stability of the PM6:IT-4F solar cells.

## 2. Results and Discussion

### 2.1. ZnO Layer Dependent Performance Decay of Inverted Solar Cells

To understand the influence of ZnO layer on the degradation processes of the solar cells, we fabricated and tested the PM6:IT-4F cells with an inverted structure of ITO/ZnO/PM6:IT-4F/MoO<sub>3</sub>/Al (Figure 1a). Three different ZnO layers were used as the ETL, including sol-gel ZnO (noted as Sg-ZnO),<sup>[10]</sup> ZnO nanoparticles synthesized by the precipitation method from methanol (MeOH) solution (noted as Me-ZnO),<sup>[11]</sup> and from dimethyl sulfoxide (DMSO) solution (noted as DMSO-ZnO; see Experimental Section for more details).<sup>[12]</sup> Figure 1b shows the UV-vis absorption spectra of the three different ZnO films deposited on the glass substrate. As seen here, the Me-ZnO showed a sharp absorption in the ultraviolet region with an absorption cut-off ( $\lambda_{\text{abs}}^{\text{cut-off}}$ ) of 400 nm, in good agreement with the results reported in the literature.<sup>[11]</sup> However, the Sg-ZnO and DMSO-ZnO show a long tailing absorption band up to 700 nm. Munirah et al. proposed that the tailing absorption band of ZnO may arise due to two main factors: one is the defect states (Tamm-Shockley states and dangling bonds), and the other one is the absorbed surface impurities (acetate arising from the sample preparation of ZnO).<sup>[13]</sup> To verify whether the broadening of ZnO absorption ( $\approx 700$  nm) is related to impurities, we performed the X-ray photoelectron spectroscopy (XPS) characterization of these ZnO films prepared by a method identical to that for the preparation of solar cells. Figure S1a, Supporting

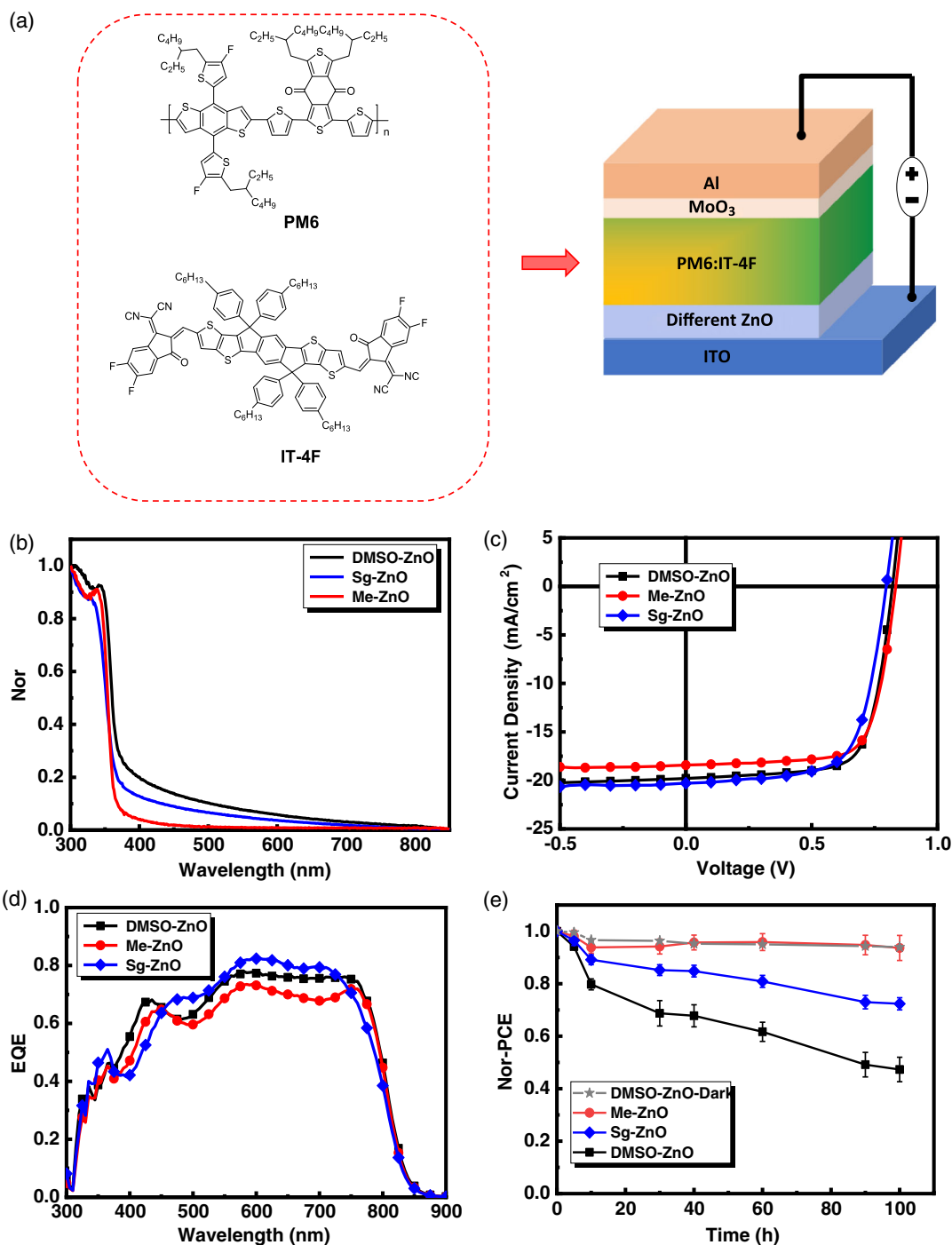


**Figure 1.** a) Solar cell device structure and molecule structures of active layer materials; b) UV-vis absorption spectra of the three different ZnO films deposited on a glass substrate; c) J-V curves and d) EQE spectra of PM6:IT-4F cells with different ZnO layer; e) PCE decay curves of PM6:IT-4F cells with different ZnO layers under white light illumination.

Information shows the complete XPS spectra of the three different ZnO films. As seen here, except for Zn 2p (1020–1045 eV), the relative intensive peaks include O 1s (528–534 eV) Zn L3MM (450–480 eV) Zn L2MM (480–510 eV) Zn 3s (120–150 eV), Zn 3p (70–100 eV) Zn 3d (0–15 eV) were also measured. However, there is no apparent difference between these three ZnO films,

suggesting that the chemical components are almost identical for these films. We then measured the high-resolution XPS spectra of the C 1s, N 1s, and Zn 2p spectra (Figure S1b–f, Supporting Information). For the C 1s spectra, broad XPS peaks were detected in all ZnO films, and the signals of O–C=O (288.5 eV), C–O (286.4 eV), and C–C (284.8 eV) can be

deduced.<sup>[14]</sup> In all cases, the O–C=O signal is relatively strong, which can be attributed to the residual acetate anions on the ZnO surface. Figure S2, Supporting Information shows the Fourier-transform infrared (FT-IR) spectroscopy of the films. The observation of the asymmetrical and symmetrical stretching of the acetate group (1581 and 1417 cm<sup>-1</sup>) in different ZnO films corresponds to the residual acetate from Zn(OAc)<sub>2</sub>. For the Sg-ZnO film, as ethanolamine was used as precursor, intensive C 1s signal of C–N bond and N1s can be clearly seen. However, this is not the reason for the lower tailing absorption band of Sg-ZnO film, as Me-ZnO showed even lower tailing absorption, although Me-ZnO did not show intensive C–N signal. Although the influence of impurity on the absorption spectrum of the ZnO films can not be completely excluded, we think that internal defects within the ZnO film should be the main reason causing the absorption differences for these ZnO films. Compared with the other two ZnO films, the DMSO-ZnO shows a more intensive absorption band over the visible light range, suggesting that ZnO nanoparticles synthesized from DMSO solution have more defect states. In addition, DMSO-ZnO exhibits the strongest photoluminescence (PL) band centered at 535 nm originating from defect states (Figure S3, Supporting Information), which further proves the aforementioned conclusion.<sup>[13]</sup> The light absorption difference of ZnO films makes them good candidates in understanding the ZnO-dependent degradation behaviors of PSCs.

The current density–voltage (*J*–*V*) characteristics and external quantum efficiency (EQE) spectra of the PSCs under AM 1.5G simulated solar illumination are shown in Figure 1c,d, respectively. The photovoltaic (PV) performance data are listed in Table 1. As seen here, all these cells show averaged PCE of 10.8–11.3%, which is comparable to the literature reported PCE for the same device structure,<sup>[16]</sup> indicating the devices are well optimized and suitable for stability comparison. All these cells were then aged inside the glovebox (with H<sub>2</sub>O < 10 ppm, O<sub>2</sub> < 10 ppm) with continuous light illumination. A white LED light (see Figure S4, Supporting Information for the spectrum of the light source) was used as the aging light source to exclude the influence of UV light. The device performance of the cells was checked under standard AM1.5G light illumination from time to time. The performance of a reference DMSO-ZnO-based cell kept in the dark was also measured for comparison. Figure 1e shows the PCE decay curves of these cells. The complete decay trace of the PV performance of these cells are shown in Figure S5, Supporting Information. As seen here, the reference DMSO-ZnO based cells kept in the dark and the Me-ZnO-based cells under white-light illumination showed almost no performance decay over 100 h, whereas the PCEs of

the DMSO-ZnO and Sg-ZnO-based cells were reduced to 42% and 72% of their initial values after aged for 100 h. The decrease in the device performance is mainly attributed to the reduced *J*<sub>sc</sub> values, whereas *V*<sub>oc</sub> and FF are relatively stable during aging (Figure S5, Supporting Information). Interestingly, the more intensive light absorption ability of ZnO layer, the faster the PV performance decays. Knowing that the PM6:IT-4F photoactive layer absorbs light cover 400–800 nm (Figure S4, Supporting Information), the observed ZnO layer depended degradation behaviors suggests that light absorption of ZnO should be the main reason for the performance decay, while the light absorption of the photoactive layer showed a negligible influence on the performance decay.

## 2.2. Interfacial Degradation of NFA Under White-Light Illumination

Zhou and Park et al. reported that UV light illumination causes the interface photochemical reaction between ZnO and the acceptor molecules and leads to the photobleaching of acceptor molecules.<sup>[7,8]</sup> To confirm that the interfacial decomposition of IT-4F at the DMSO-ZnO/IT-4F interface happens as well under white-light illumination, DMSO-ZnO/PM6:IT-4F, DMSO-ZnO/IT-4F, DMSO-ZnO/PM6, and IT-4F films on glass were aged under LED white light, and the UV-vis absorption spectra of the films were recorded from time to time. Figure 2a and Figure S6, Supporting Information show the absorption spectra changes of these films upon aging. As seen here, absorption of IT-4F component (600–800 nm) decreases gradually for the DMSO-ZnO/IT-4F (Figure 2a), DMSO-ZnO/PM6:IT-4F (Figure S6a, Supporting Information) films with the increase in light-soaking time. In contrast, no significant change was observed either for the DMSO-ZnO/PM6 nor the IT-4F-only films (Figure S6b,c, Supporting Information), indicating that only IT-4F showed photobleaching process at the ZnO interface. Note that no absorption spectrum change was measured for the DMSO-ZnO/IT-4F film when the film was kept in the dark (Figure S6d, Supporting Information), indicating that light illumination is essential for the interfacial degradation of IT-4F on DMSO-ZnO surface.

We then compared the photobleaching process of IT-4F on different ZnO surfaces. The absorption spectra of Me-ZnO/IT-4F and Sg-ZnO/IT-4F films under light soaking are shown in Figure 2b,c, respectively. Figure 2d compares the decrease in the absorbance of the IT-4F component on different ZnO, and the photobleaching rate of IT-4F is directly correlated to the light-absorption ability of the ZnO layer in the visible light range. These results confirmed again that light absorption of ZnO is the essential step for the interfacial degradation of the acceptor molecule, while light absorption of the organic component has a negligible influence on the interfacial decomposition.

## 2.3. Product Analysis of the Photobleached Films

To verify the detailed photochemical reaction at the ZnO/IT-4F interface, the products of the ZnO/IT-4F film after light illumination were measured by MALDI-TOF-MS. Figure 3 shows the MS spectrometry of the initial IT-4F and the products of the films

**Table 1.** Performance of devices based on PM6:IT-4F with different ZnO.

CIL	<i>V</i> <sub>oc</sub> [V]	<i>J</i> <sub>sc</sub> [mA cm <sup>-2</sup> ]	FF	PCE [%] <sup>a)</sup>	PCE <sub>max</sub> [%] <sup>b)</sup>
DMSO-ZnO <sup>a)</sup>	0.82 ± 0.004	19.64 ± 0.219	0.71 ± 0.017	11.33 ± 0.191	11.52
Me-ZnO	0.83 ± 0.004	18.39 ± 0.094	0.72 ± 0.009	11.03 ± 0.118	11.20
Sg-ZnO	0.80 ± 0.006	20.35 ± 0.083	0.67 ± 0.003	10.84 ± 0.057	10.95

<sup>a)</sup>Averaged device performance over 8 individual cells; <sup>b)</sup>PCE of the best cell.

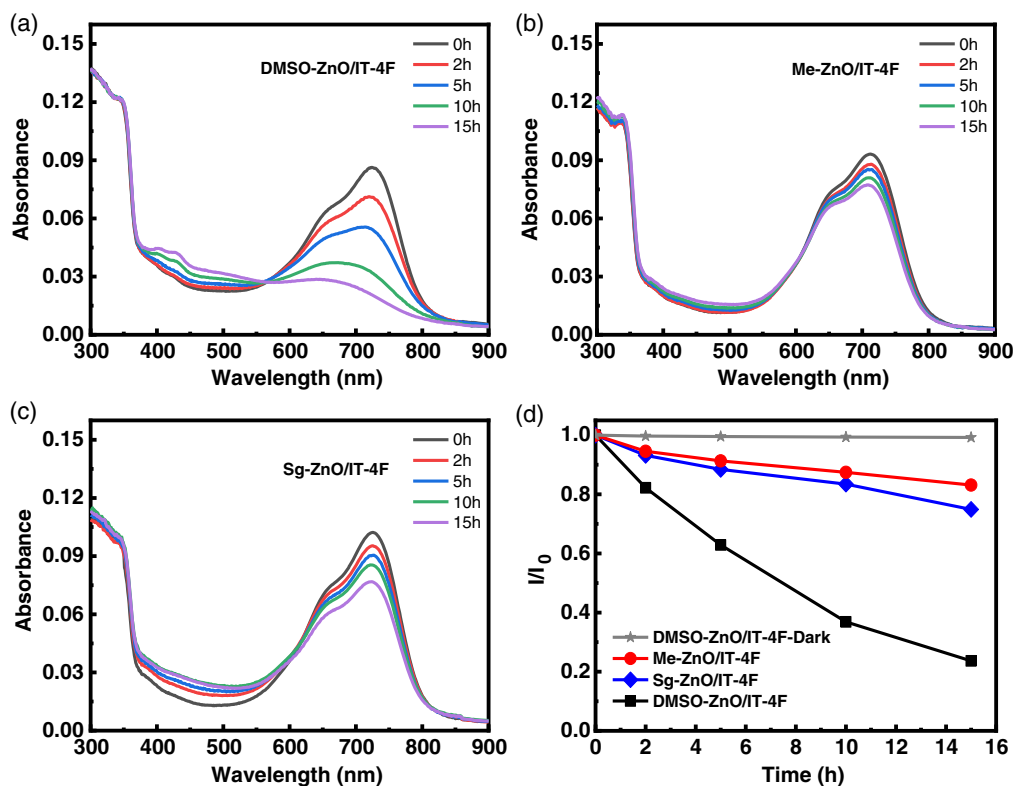


**Figure 2.** UV-vis absorption spectra of a) DMSO-ZnO/IT-4F; b) Me-ZnO/IT-4F; c) Sg-ZnO/IT-4F films under white-light illumination; d) The decrease in the absorbance of the IT-4F component on different ZnO surface.

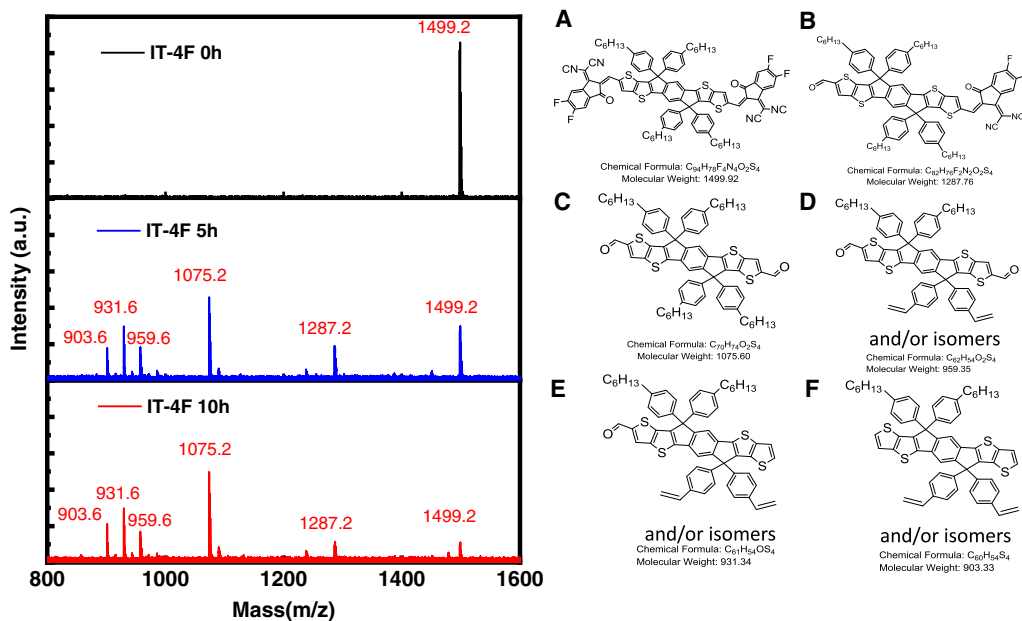


**Figure 3.** MALDI-MS spectra of the pristine IT-4F and the products of the aged IT-4F on DMSO-ZnO surface.

after illuminated for 5 and 10 h. As seen here, the initial IT-4F (compound A in Figure 3) sample showed an MS peak at  $m/z$  of 1499.16, corresponding to the  $M + H^+$  of IT-4F molecule. After illuminated for 5 h, five MS signals were measured peaking at

1287.2, 1075.2, 959.6, 931.6, and 903.6. The first two MS signals can be attributed to the decoupled products with mono- or bis-aldehyde groups (compound B and C in Figure 3), which means the C=C bond linking the donor (IDTT) and acceptor (EG-2F)

moieties in IT-4F was broken (see Figure S7, Supporting Information for the decoupling reaction). The other three sets of signals are then assigned to the styrene-containing products that originate from the dealkylation of the hexyl chain (product D, E, and F in Figure 3, and Figure S7, Supporting Information for the dealkylation reaction). Decrease in the relative intensity of the MS signal of IT-4F and B was observed for the film aged for 10 h, indicating the decomposition of IT-4F with the increase in light illumination time, which is in good accordance with the decrease in light absorbance of IT-4F under light illumination (Figure 2a).

#### 2.4. The Photochemical Reaction of IT-4F on ZnO Surface

The detection of dealkylated products in the aged ZnO/IT-4F film suggests that the reactive species causing the decomposition of IT-4F must be radicals. In combination with the detection of mono- and bis-aldehyde products (compound B and C in Figure 3), hydroxyl radicals ( $\bullet\text{OH}$ ) were supposed to be the main reactive species. To prove this, ESR was performed on the ZnO film with or without white light illumination (see Experimental Section for more details). Figure 4a shows the ESR spectra of

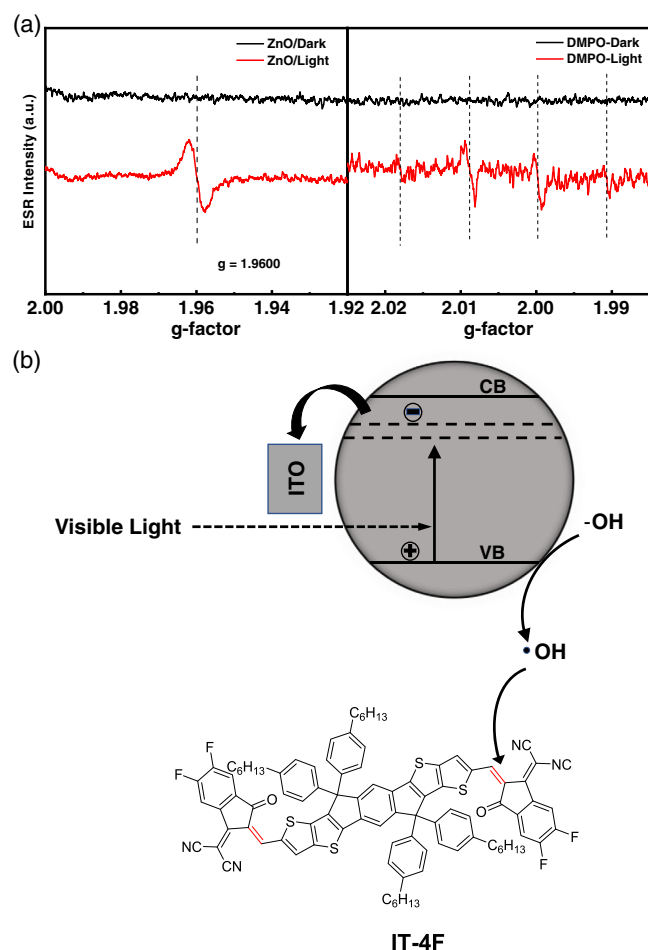


**Figure 4.** a) ESR of ZnO film with and without white-light illumination; DMPO solution extracted from the ZnO film before and after light illumination; b) Proposed white-light-induced interfacial degradation mechanism between ZnO and IT-4F.

ZnO film. As seen here, no ESR signal was detected for the ZnO film in the dark, whereas a broad ESR resonance peak with a  $g$  value of 1.9600 was measured for the same film under light illumination, which is attributed to the formation of oxygen vacancies ( $\text{V}_{\text{O}}^+$ ).<sup>[17]</sup> To confirm the formation of hydroxyl radicals on the ZnO surface, we use 5,5-Dimethyl-1-pyrroline-*N*-oxide (DMPO) toluene solution as the hydroxyl radical capture reagent. The prepared ZnO film was immersed in a DMPO toluene solution in the dark, and a small portion of DMPO toluene solution was taken for ESR measurement (noted as DMPO-dark). Then the sample was illuminated with white light for 0.5 h, and another small portion of DMPO toluene solution was taken for ESR measurement again (noted as DMPO-light). Figure 4a showed the ESR spectra of these two DMPO solutions. As seen here, no ESR signal was measured for the solution without light illumination. In contrast, signals with a characteristic intensity ratio of 1:2:2:1 were measured, which are attributed to the formation of DMPO-OH adducts.<sup>[18]</sup> These results confirm the formation of hydroxyl radicals on the ZnO surface under light illumination. In addition, ESR spectra (Figure S8, Supporting Information) of DMPO with or without white-light illumination were measured for comparison. The results show that no ESR signals were detected in DMPO no matter under dark or light. Note that the ZnO layer was annealed at 130 °C for 10 min during the cell preparation, and the complete cells were aged inside the glovebox with low water and moisture content ( $\text{H}_2\text{O} < 10$  ppm,  $\text{O}_2 < 10$  ppm). The formation of hydroxyl radicals is more possibly due to the oxidation of the dangling hydroxide groups ( $\text{OH}^-$ )<sup>[19]</sup> on the ZnO surface rather than the oxidation of oxygen and/or  $\text{H}_2\text{O}$  as proposed by Park and Son.<sup>[8]</sup> Therefore, a mechanism for the photon-induced degradation of IT-4F by ZnO is proposed (Figure 4b), which includes the following steps. 1) The existence of ZnO defect states enhances the light absorption of ZnO in visible light; 2) light absorption of ZnO creates holes in the valence band and electrons in the conduction band; 3) the dangling  $\text{OH}^-$  is oxidized by the holes and generate reactive hydroxyl radicals; 4) decomposition of IT-4F molecule by hydroxyl radicals through decoupling reactions as shown in Figure S7, Supporting Information.

#### 2.5. Suppression of Interfacial Decomposition by Surface Treatment

As the hydroxyl radicals are generated by the photo-induced oxidation of hydroxide by ZnO, treating the ZnO surface with hydroxide or hydroxyl scavengers is expected to be able to suppress the decomposition of IT-4F and consequently improve the stability of the PSCs. Different chemicals, including alcohol (MeOH and isopropyl alcohol [IPA] as weak acid), 2-phenylethanthiol (PET), as well as ethylenediaminetetraacetic acid (EDTA) were used to modify the ZnO surface. Figure 5a and Figure S9, Supporting Information show the  $J$ - $V$  characteristics and EQE spectra of these cells with the modified ZnO layer, respectively, and the PV performance data are listed in Table S1, Supporting Information. Although the concentration of the surface modifier was not fully optimized, all these PM6:IT-4F cells showed PCE of 11–12%, which are comparable to the reference cells (Table 1), suggesting the surface treatment with these reagents does not

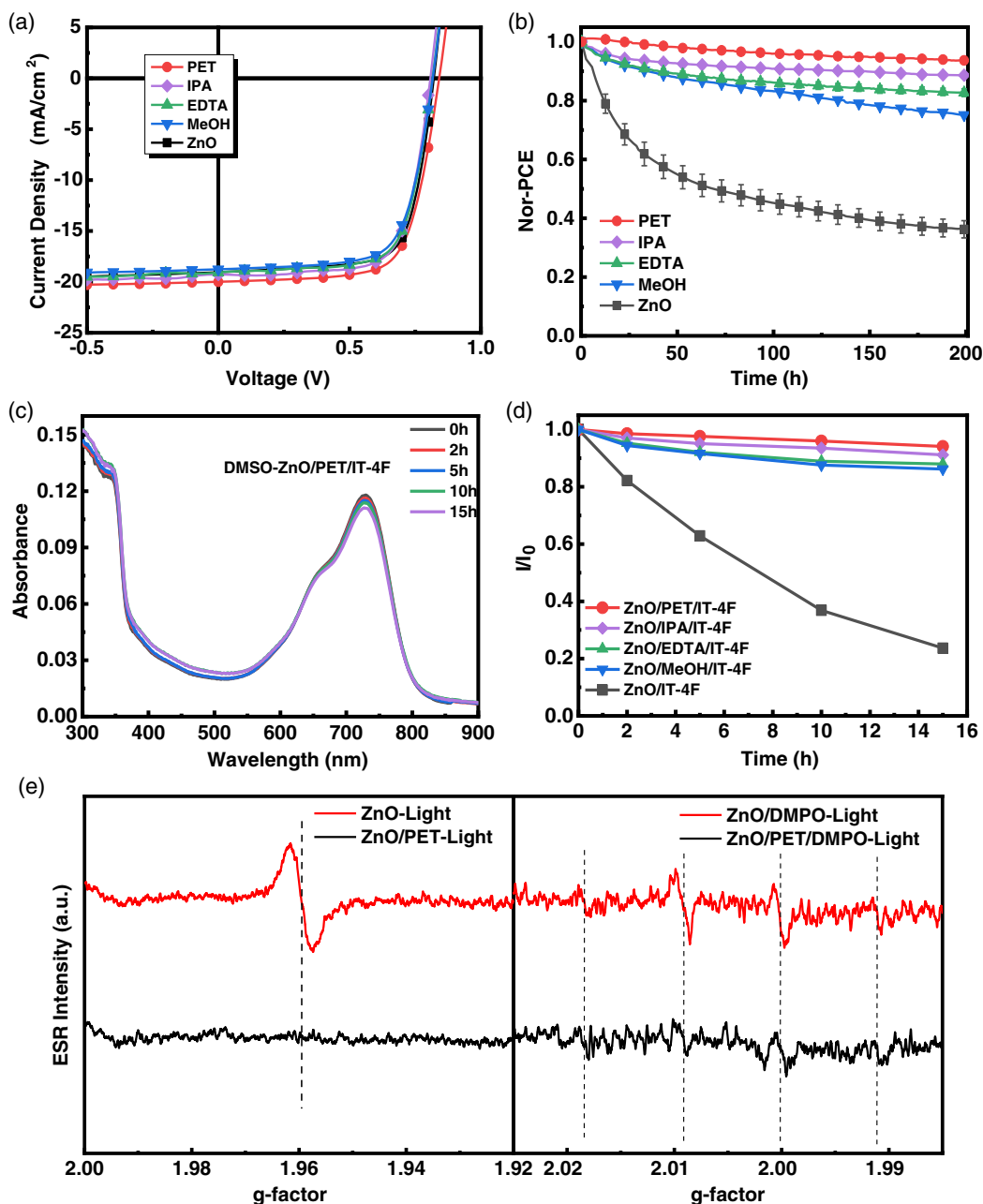


**Figure 5.** a)  $J$ - $V$  curves of PSCs based on surface-treated ZnO layers; b) PCE decay curves of PM6:IT-4F cells with surface treatment under white-light illumination; c) UV-vis absorption spectra of IT-4F film on ZnO modified by PET; d) Decay rate of absorption of IT-4F thin films on surface-treated ZnO layers; e) ESR spectra of ZnO film with or without PET modified under white-light illumination; ESR spectra of DMPO solution extracted from the ZnO film and ZnO/PET film after light illumination.

influence the device performance significantly. However, as seen in Figure 5b, all these cells showed significant stability improvement after surface treatment (see Figure S10, Supporting Information for the complete PV performance decay curves).

To prove that surface treatment of the ZnO layer improves the stability of the devices by suppressing the interfacial photochemical reaction, thin films with a structure of ITO/ZnO/IT-4F and ITO/ZnO/surface modifier/IT-4F were fabricated and aged under white-light illumination. The UV-vis absorption spectra

of these films were then recorded, and the results are shown in Figure 5c and Figure S11, Supporting Information. Figure 5d shows the absorption changes of IT-4F thin films on the surface PET-treated ZnO layer. Compared with the ZnO/IT-4F film, the absorption changes in ZnO/PET/IT-4F film have slowed down clearly after the surface treatment, corresponding well to the device stability improvement results.

Figure 5e shows the ESR spectra of pristine and PET-modified ZnO films with or without light illumination. As seen here, the

signal of oxygen vacancy of ZnO under light illumination vanished after surface treatment with PET. Also, almost no signal was detected for DMPO toluene solution extracted from the DMSO–ZnO/PET film under light illumination, suggesting that surface treatment of ZnO with PET suppresses the forming of hydroxyl radicals. Note that absorption of the DMSO–ZnO after PET treatment does not show much difference to the pristine one (Figure S12, Supporting Information). The suppression effect of PET should not be due to the change of sub-band of ZnO, but more related to the blocking of photon-induced generation of hydroxyl radicals.

### 3. Conclusion

In summary, three different ZnO layers with different light-absorption capability were prepared and used for the PM6:IT-4F solar-cell degradation mechanism study. Using UV-free LED light as the light source, we confirmed that the PV performance decay rate of the cells is directly related to the light absorption ability of ZnO in the visible light range. In addition, photobleaching was only measured for the IT-4F containing organic films on ZnO surface, confirming that light absorption of ZnO is the first essential step for the degradation of the cells. ESR and MALDI-TOF-MS analyses on the ZnO and ZnO/IT-4F film with or without light illumination proved that hydroxyl radicals are the reactive species that decompose the acceptor molecules. Therefore, the interfacial degradation of NFA molecule is proposed to be due to the formation of hydroxyl radicals that come from the oxidation of the dangling hydroxyl group by the holes in the valance band flowing the light absorption of ZnO layer. Finally, we found out that surface treatment of ZnO with hydroxide and hydroxyl radical scavengers can successfully improve the stability of the cells, which further supports the proposed degradation mechanism.

### 4. Experimental Section

**Materials:** PM6 (PBDB-T-2F) and IT-4F were purchased from Solarmer Materials Inc, Beijing. PET, Zn(OAc)<sub>2</sub>, tetramethylammonium hydroxide (TMAH), chlorobenzene (CB, 99.8%) were purchased from J&K Scientific Ltd. IPA, EDTA, MeOH were purchased from MACKLIN. DIO was purchased from Sigma-Aldrich. DMPO was purchased from Dojindo. Molybdenum (VI) oxide (MoO<sub>3</sub>) was purchased from Strem Chemicals. All materials were used as received without further purification. Me-ZnO nanoparticles solution was prepared through the reaction between KOH and Zn(OAc)<sub>2</sub> in MeOH as reported by Beek et al.<sup>[11]</sup> DMSO–ZnO was prepared through the reaction between TMAH and Zn(OAc)<sub>2</sub> in DMSO as reported by Qian et al.<sup>[12]</sup> Sg-ZnO precursor solution was prepared by dissolving 148 mg of zinc acetate in 80 μL of ethanolamine and 1.5 mL of 2-methoxyethanol as reported by Sun et al.<sup>[10]</sup>

**Instruments and Measurement:** The ultraviolet–visible (UV–Vis) absorption spectra of ZnO and IT-4F films were measured with a PerkinElmer Lambda 750 at room temperature. All the films were spin-coated on the glass substrates and aged in glovebox under white LED light. The mass spectra of IT-4F were measured with MALDI-TOF-MS. IT-4F were spin-coated on the glass substrates and degraded in white LED light for 5 and 10 h. Then the degraded films were dissolved with methylene chloride (CH<sub>2</sub>Cl<sub>2</sub>) and dried under vacuum. ESR of the ZnO films was performed with an ESR spectrometer (JEOL JES-X320). The samples for ESR measurement were prepared by putting the solution of ZnO in ethanol (200 μL, 10 mg mL<sup>-1</sup>) into a standard 5 mm NMR tube, and the solvent was then

removed under vacuum, finally annealed at 130 °C for 10 min on a hot plate in a glove box filled with N<sub>2</sub>. The measurements were carried out at room temperature with or without white light illumination from a LED lamp (400–800 nm). The formation of hydroxyl radicals was detected with spin trapping measurements coupled with ESR spectroscopy. DMPO solution (100 mmol L<sup>-1</sup> in toluene) was added as a spin-trapping agent of ·OH to the ZnO film spin-coated on the glass substrates in bottles under white light for 30 min in glove box filled with N<sub>2</sub>. The DMPO solution extracted from ZnO film with 0.5 mm capillary were carried out at room temperature. ZnO NPs solutions (DMSO–ZnO and Me–ZnO 10 mg mL<sup>-1</sup> in ethanol) were spin-coated on the ITO substrates and then were annealed on a hot plate in glove box. Sg–ZnO was also spin-coated on the ITO substrates but was annealed on a hot plate in air. The samples were put into a N<sub>2</sub>-filled chamber and transferred to the vacuum chamber for XPS testing as careful as possible to minimize the undesired contamination. The different ZnO films were prepared on the glass substrates as described earlier and their PL spectra were measured by utilizing a F-4600 FL spectrophotometer with excitation at 320 nm, entrance slit: 10 nm bandpass, exit slit: 10 nm, integration time 0.1 s. The different ZnO films for FT-IR measurement were prepared on CaF<sub>2</sub> surface according to the identical procedure for solar cell fabrication. The FT-IR spectra were measured on a Nicolet 6700 FT-IR spectrometer.

**Fabrication of PSCs:** ITO substrates were sequentially cleaned by detergent, deionized water, acetone, and isopropanol in ultrasound cleaner. Then they were put in the isopropanol for storage. Before using them, they were first dried by N<sub>2</sub> flow and then treated in a UV–ozone oven for 30 min. First, ZnO NPs (DMSO–ZnO and Me–ZnO 10 mg mL<sup>-1</sup> in ethanol) was spin-coated on the ITO substrates at 2000 rpm for 60 s and then were annealed at 130 °C for 10 min on a hot plate in glove box filled with N<sub>2</sub>. S-g ZnO was also spin-coated on the ITO substrates at 2000 rpm for 60 s but was annealed at 130 °C for 30 min on a hot plate in air. The solution of PM6:IT-4F (10 mg mL<sup>-1</sup> for each compound) blended in CB was spin-coated on the top of the ZnO ETL at 2000 rpm for 60 s and then were annealed at 130 °C for 10 min on a hot plate in glove box filled with N<sub>2</sub>. Finally, MoO<sub>3</sub> (20 nm) as the hole-extraction layer and Al (100 nm) as the anode were sequentially vacuum-deposited on the top of the active layer, respectively. In addition, the surface treatment of ZnO was that the solution of modifier was spin-coated on the top of the ZnO ETL at 3000 rpm for 30 s and then were annealed at 130 °C for 5 min on a hot plate in glove box filled with N<sub>2</sub>. The effective PV area, defined by the geometrical overlap between the bottom cathode electrode and the top anode, was 0.09 cm<sup>2</sup>.

**PV Parameters of PSCs:** The PV parameters of the cells including V<sub>oc</sub>, J<sub>sc</sub>, and FF were measured using a Keithley 2400 source meter under illumination with simulated AM 1.5G sunlight (Verasol-2, LED 3A Sun Simulator, Newport) in a glove box filled with N<sub>2</sub>. The EQE spectra were recorded by EQE system which was built in home and the light from a 150 W tungsten halogen lamp (Osram 64610) was used as a probe light and was modulated with a mechanical chopper before passing through the monochromator (Zolix, Omni-k300) to select the wavelength. The response was recorded as the voltage by an I–V converter (D&R-IV Converter, Suzhou D&R Instruments), using a lock-in amplifier (Stanford Research Systems SR 830). A stand silicon cell was used as the reference before testing the devices.

**Degradation of PSCs Under White Light:** The long-term stability of unencapsulated devices was conducted by multi-channel solar cell performance decay test system (PVL-T-G8001M, Suzhou D&R Instruments Co. Ltd.) under a testing condition in accordance with ISOS-L-1<sup>[20]</sup> in the glove box. The cells were put inside a glove box filled with N<sub>2</sub> (H<sub>2</sub>O < 10 ppm, O<sub>2</sub> < 10 ppm) and continuously illuminated with white LED light (D&R Light, L-W5300KA-150, Suzhou D&R Instruments). The illumination light intensity was initially set so the output short-circuit current density (J<sub>sc</sub>) is as same as that measured under standard conditions by AM1.5G. For monitoring changes in illumination light intensity, it was monitored by a photodiode (Hamamatsu S1336-8BQ). J–V characters of the devices were checked periodically, and the PV performances data (V<sub>oc</sub>, J<sub>sc</sub>, FF, and PCE) were calculated automatically according to the J–V curves. When J–V was tested, an external load matching the maximum power output



point ( $R_{mpp} = V_{max}/I_{max}$ ), was attached to the cell. So, the performance of devices can be recorded automatically with time to monitor the  $J-V$  curves. Because external load can be changed with the  $J-V$  results, the measured performance decay curves means the performance decay behavior of cells under real operation. It is clear that the results fully achieved the highest level of ISOS-L3. The temperature of the cells is thermostatically controlled at room temperature 25 °C by temperature control equipment.

## Supporting Information

Supporting Information is available from the Wiley Online Library or from the author.

## Acknowledgements

The authors acknowledge the financial support from the Ministry of Science and Technology of China (no. 2016YFA0200700), the National Natural Science Foundation of China (61904121, 21571019), Chinese Academy of Science (no. YJKYYQ20180029, CAS-ITRI 2019010, GJHZ2092-019), Youth Innovation Promotion Association of (CAS 2019317), Natural Science Foundation of Shanxi Province (201801D221136).

## Conflict of Interest

The authors declare no conflict of interest.

## Keywords

degradation and stability, hydroxyl radicals, interface degradation, photochemical reactions, polymer solar cells

Received: October 10, 2020  
Revised: November 13, 2020  
Published online:

- [1] a) Y. Li, G. Xu, C. Cui, Y. Li, *Adv. Energy Mater.* **2018**, *8*, 1701791; b) G. Li, R. Zhu, Y. Yang, *Nat. Photonics* **2012**, *6*, 153; c) S. R. Forrest, *Nature* **2004**, *428*, 911; d) K. Zhang, Z. Hu, C. Sun, Z. Wu, F. Huang, Y. Cao, *Chem. Mater.* **2017**, *29*, 141; e) R. Xue, J. Zhang, Y. Li, Y. Li, *Small* **2018**, *14*, 1801793.
- [2] a) G. Zhang, J. Zhao, P. C. Y. Chow, K. Jiang, J. Zhang, Z. Zhu, J. Zhang, F. Huang, H. Yan, *Chem. Rev.* **2018**, *118*, 3447; b) P. Cheng, G. Li, X. Zhan, Y. Yang, *Nat. Photonics* **2018**, *12*, 131; c) W. Zhao, D. Qian, S. Zhang, S. Li, O. Inganäs, F. Gao, J. Hou, *Adv. Mater.* **2016**, *28*, 4734; d) Y. Cui, H. Yao, J. Zhang, T. Zhang, Y. Wang, L. Hong, K. Xian, B. Xu, S. Zhang, J. Peng, Z. Wei, F. Gao, J. Hou, *Nat. Commun.* **2019**, *10*, 2515.
- [3] a) A. Wadsworth, M. Moser, A. Marks, M. S. Little, N. Gasparini, C. J. Brabec, D. Baran, I. McCulloch, *Chem. Soc. Rev.* **2019**, *48*, 1596; b) C. Yan, S. Barlow, Z. Wang, H. Yan, A. K. Y. Jen, S. R. Marder, X. Zhan, *Nat. Rev. Mater.* **2018**, *3*, 18003; c) C. B. Nielsen, S. Holliday, H.-Y. Chen, S. J. Cryer, I. McCulloch, *Acc. Chem. Res.* **2015**, *48*, 2803; d) J. Hou, O. Inganäs, R. H. Friend, F. Gao, *Nat. Mater.* **2018**, *17*, 119.
- [4] a) Q. Liu, Y. Jiang, K. Jin, J. Qin, J. Xu, W. Li, J. Xiong, J. Liu, Z. Xiao, K. Sun, S. Yang, X. Zhang, L. Ding, *Sci. Bull.* **2020**, *65*, 272; b) Y. Lin, Y. Firdaus, F. H. Isikgor, M. I. Nugraha, E. Yengel, G. T. Harrison, R. Hallani, A. El-Labban, H. Faber, C. Ma, X. Zheng, A. Subbiah, C. T. Howells, O. M. Bakr, I. McCulloch, S. D. Wolf, L. Tsetseris, T. D. Anthopoulos, *ACS. Energy Lett.* **2020**, *5*, 2935.
- [5] a) H. Kang, G. Kim, J. Kim, S. Kwon, H. Kim, K. Lee, *Adv. Mater.* **2016**, *28*, 7821; b) E. M. Speller, A. J. Clarke, J. Luke, H. K. H. Lee, J. R. Durrant, N. Li, T. Wang, H. C. Wong, J. S. Kim, W. C. Tsoi, Z. Li, *J. Mater. Chem. A* **2019**, *7*, 23361.
- [6] a) C. Wang, S. F. Ni, S. Braun, M. Fahlman, X. J. Liu, *J. Mater. Chem. C* **2019**, *7*, 879; b) N. Gasparini, M. Salvador, S. Strohm, T. Heumueller, I. Levchuk, A. Wadsworth, J. H. Bannock, J. C. de Mello, H.-J. Egelhaaf, D. Baran, I. McCulloch, C. J. Brabec, *Adv. Energy Mater.* **2017**, *7*, 1700770; c) Y. Xin, G. Zeng, J. Y. OuYang, X. L. Zhao, X. N. Yang, *J. Mater. Chem. C* **2019**, *7*, 9513; d) X. Du, T. Heumueller, W. Gruber, A. Classen, T. Unruh, N. Li, C. J. Brabec, *Joule* **2019**, *3*, 215; e) A. Classen, T. Heumueller, I. Wabra, J. Gerner, Y. He, L. Einsiedler, N. Li, G. J. Matt, A. Osvet, X. Du, A. Hirsch, C. J. Brabec, *Adv. Energy Mater.* **2019**, *9*, 1902124; f) J. Luke, E. M. Speller, A. Wadsworth, M. F. Wyatt, S. Dimitrov, H. K. H. Lee, Z. Li, W. C. Tsoi, I. McCulloch, D. Bagnis, J. R. Durrant, J.-S. Kim, *Adv. Energy Mater.* **2019**, *9*, 1803755; g) Y. Wang, W. Lan, N. Li, Z. Lan, Z. Li, J. Jia, F. Zhu, *Adv. Energy Mater.* **2019**, *9*, 1900157.
- [7] Y. Y. Jiang, L. L. Sun, F. Y. Jiang, C. Xie, L. Hu, X. Y. Dong, F. Qin, T. F. Liu, L. Hu, X. S. Jiang, Y. H. Zhou, *Mater. Horizons* **2019**, *6*, 1438.
- [8] S. Park, H. J. Son, *J. Mater. Chem. A* **2019**, *7*, 25830.
- [9] X. Xu, J. Xiao, G. Zhang, L. Wei, X. Jiao, H.-L. Yip, Y. Cao, *Sci. Bull.* **2020**, *65*, 208.
- [10] Y. Sun, J. H. Seo, C. J. Takacs, J. Seifert, A. J. Heeger, *Adv. Mater.* **2011**, *23*, 1679.
- [11] W. J. E. Beek, M. M. Wienk, M. Kemerink, X. Yang, R. A. J. Janssen, *J. Phys. Chem. B* **2005**, *109*, 9505.
- [12] L. Qian, Y. Zheng, K. R. Choudhury, D. Bera, F. So, J. Xue, P. H. Holloway, *Nano Today* **2010**, *5*, 384.
- [13] Munirah Z. R. Khan, A. Aziz, M. S. Khan, M. U. Khandaker, *Mater. Sci-Poland* **2017**, *35*, 246.
- [14] S. B. Amor, M. Jacquet, P. Fioux, M. Nardin, *Appl. Surf. Sci.* **2009**, *255*, 5052.
- [15] C. Chandrinou, N. Boukos, C. Stogios, A. Travlos, *Microelectron. J.* **2009**, *40*, 296.
- [16] a) Q. Fan, W. Su, Y. Wang, B. Guo, Y. Jiang, X. Guo, F. Liu, T. P. Russell, M. Zhang, Y. Li, *Sci. China Chem.* **2018**, *61*, 531; b) X. Zhu, B. Guo, J. Fang, T. Zhai, Y. Wang, G. Li, J. Zhang, Z. Wei, S. Duhm, X. Guo, M. Zhang, Y. Li, *Org. Electron.* **2019**, *70*, 25; c) S. Zhang, Y. Qin, J. Zhu, J. Hou, *Adv. Mater.* **2018**, *30*, 1800868.
- [17] a) L. Zhang, L. Yin, C. Wang, N. lun, Y. Qi, D. Xiang, *J. Phys. Chem. C* **2010**, *114*, 9651; b) P. Jakes, E. Erdem, *Phys. Status Solidi-R* **2011**, *5*, 56; c) V. Ischenko, S. Polarz, D. Grote, V. Stavarache, K. Fink, M. Driess, *Adv. Funct. Mater.* **2005**, *15*, 1945.
- [18] a) J. R. Harbour, M. L. Hair, *J. Phys. Chem.* **1979**, *83*, 652; b) A. Lipovsky, Z. Tzitrinovich, H. Friedmann, G. Applerot, A. Gedanken, R. Lubart, *J. Phys. Chem. C* **2009**, *113*, 15997; c) G. D. Feng, P. Cheng, W. F. Yan, M. Boronat, X. Li, J. H. Su, J. Y. Wang, Y. Li, A. Corma, R. R. Xu, J. H. Yu, *Science* **2016**, *351*, 1188.
- [19] a) N. M. Mahmoodi, M. Arami, N. Y. Limaee, N. S. Tabrizi, *J. Colloid. Interface Sci.* **2006**, *295*, 159; b) M. A. Rauf, S. S. Ashraf, *Chem. Eng. J.* **2009**, *151*, 10; c) F. C. Krebs, Y. Thomann, R. Thomann, J. W. Andreasen, *Nanotechnology* **2008**, *19*, 424013; d) A. Abdolmaleki, S. Mallakpour, S. Borandeh, *Polym. Bull.* **2012**, *69*, 15.
- [20] M. V. Khenkin, E. A. Katz, A. Abate, G. Bardizza, J. J. Berry, C. Brabec, F. Brunetti, V. Bulović, Q. Burlingame, A. Di Carlo, R. Cheacharoen,

Y.-B. Cheng, A. Colsmann, S. Cros, K. Domanski, M. Dusza, C. J. Fell, S. R. Forrest, Y. Galagan, D. Di Girolamo, M. Grätzel, A. Hagfeldt, E. von Hauff, H. Hoppe, J. Kettle, H. Köbler, M. S. Leite, S. Liu, Y.-L. Loo, J. M. Luther, C.-Q. Ma, M. Madsen, M. Manceau, M. Matheron, M. McGehee, R. Meitzner, M. K. Nazeeruddin,

A. F. Nogueira, Ç. Odabaşı, A. Osherov, N.-G. Park, M. O. Reese, F. De Rossi, M. Saliba, U. S. Schubert, H. J. Snaith, S. D. Stranks, W. Tress, P. A. Troshin, V. Turkovic, S. Veenstra, I. Visoly-Fisher, A. Walsh, T. Watson, H. Xie, R. Yıldırım, S. M. Zakeeruddin, K. Zhu, M. Lira-Cantu, *Nat. Energy* **2020**, *5*, 35.